PERGAMON

International Journal of Solids and Structures 37 (2000) 1133–1144

INTERNATIONAL JOURNAL OF SOLIDS and STRUCTURES

www.elsevier.com/locate/ijsolstr

Intergranular squirt flow in sand: grains with viscous cement

Klaus C. Leurer, Jack Dvorkin*

Department of Geophysics, Stanford University, Stanford, CA 94305-2215, USA

Received 23 January 1998; in revised form 1 October 1998

Abstract

We offer an exact solution to the problem of deformation of two elastic spherical particles with viscous cement at their contact. This model is intended to mimic a granular geomaterial whose grains are covered with viscous fluid of geologic or biogenic nature (e.g., marine sediment, heavy-oil sand, asphalt concrete). The solution for the normal stiffness of a two-grain combination is reduced to an ordinary integro-differential equation that has to be solved numerically. We find two approximations for the rigorous numerical solution. The simplest one, based on the Maxwell viscoelastic model, cannot accurately reproduce the relaxational behavior of the system. The second one is based on the Cole–Cole model that allows one to introduce a spectrum of relaxation times. This expression is very accurate and can be used instead of the numerical solution. The complex effective elastic moduli of the aggregate are calculated from statistical averaging for a dense random pack of identical spheres. The theoretical results match well experimental data obtained on a glass bead pack with viscous epoxy cement.

1. Introduction and problem formulation

The elastic properties of a granular aggregate such as oil sand or marine sediment strongly depend on the stiffness of the grain-to-grain contacts. This stiffness can be affected by the presence of high-viscosity fluid (e.g., heavy oil, clay suspension, or a biogenic material) that envelops the grains. This fluid may act as contact cement and reinforce the intergranular contacts (Fig. 1).

The effective elastic properties of a granular aggregate with viscous cement are frequency-dependent. At zero frequency, pressure in viscous cement is equal to that in the surrounding pore space. Therefore, viscous cement will not contribute to the stiffness of the grain-to-grain contact. At infinite frequency, viscous cement becomes unrelaxed and deforms as an elastic body. Now it may strongly reinforce the

* Corresponding author. Fax: 001 650 725 7344.
E-mail address: jack@pangea.stanford.edu (J. Dvorkin).

0020-7683/00/$ - see front matter
PII: S0020-7683(98)00299-6

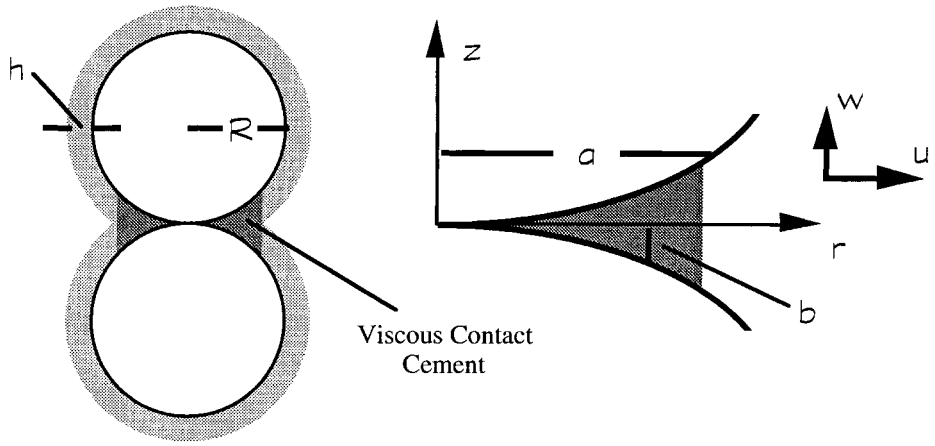

Fig. 1. Left: two spherical grains with a point direct contact enveloped by high-viscosity fluid. Right: the grain contact region with viscous contact cement.

contacts. At intermediate frequencies local (squirt) flow of viscous cement develops between the grains. Such viscous flow is responsible for velocity-frequency dispersion and attenuation (e.g., Mavko and Jizba, 1991; Dvorkin et al., 1995). Our goal is to quantitatively describe the squirt flow of viscous cement between grains and quantify its effect on the stiffness of the sediment frame and, therefore, acoustic velocity and attenuation in the sediment.

In order to solve the problem, we assume that the grains are spherical and elastic, and cement is a Newtonian compressible viscous fluid. We assume that the confining force acting on the grains is zero, i.e., the direct grain-to-grain contact is a point and the grains are in close-pack suspension. When the system is deformed by an acoustic wave, the direct grain-to-grain contact remains a point, and the external wave-induced force is counteracted by hydrodynamic pressure developed in viscous cement.

The main part of the solution is finding the normal stiffness of a two-grain combination. This normal stiffness is defined as the ratio of the applied (to the grains) normal force to the resulting increment of the displacement of the sphere center. Because the grains are not precompacted, we assume that the shear stiffness of two grains is zero.

Once the expression for the normal contact stiffness is obtained, it can be used in a numerical discrete element code. For the special case of a random close pack of identical spherical grains the following analytical expressions can be used to calculate the effective bulk (K_{Eff}) and shear (G_{Eff}) moduli of the aggregate (e.g., Dvorkin et al., 1994):

$$K_{\mathrm{Eff}} + \frac{n(1-\phi)}{12\pi R} S_{\mathrm{n}}, \quad G_{\mathrm{Eff}} = \frac{3}{5} K_{\mathrm{Eff}}; \tag{1}$$

where S_{n} is the normal stiffness between two grains; $n \approx 9$ is the coordination number (the average number of contacts per gram); $\phi \approx 0.36$ is the aggregate's porosity.

2. Governing equation

We describe the dynamics of the viscous cement by examining its flow induced by the oscillations of the grain surfaces (Dvorkin et al., 1990). Specifically, we consider oscillations at a fixed angular frequency ω. Then the half-thickness b of the cement layer in the vicinity of the point grain-to-grain

contact is a function of the radial coordinate r and time t:

$$b(r,t) = r^2/(2R) + b_0(r)\,\mathrm{e}^{i\omega t}, \tag{2}$$

where R is the grain radius, and $b_0 \ll b$ is the amplitude of the grain surface oscillations.

For an acoustic compressible fluid with the speed of sound c_0 the pressure increment $\mathrm{d}P$ is proportional to the density increment $\mathrm{d}\rho$ as

$$\mathrm{d}P = c_0^2\,\mathrm{d}\rho. \tag{3}$$

The mass conservation equation in the contact region (Fig. 1) is

$$\frac{\partial\rho}{\partial t} + \frac{\partial(\rho u)}{\partial r} + \frac{\rho u}{r} + \frac{\partial(\rho w)}{\partial z} = 0, \tag{4}$$

where u is the velocity component along the r-coordinate, and w is the velocity component along the z-coordinate.

Let us integrate eqn (4) in the z-direction from 0 to b and take into account that

$$w = 0, \quad z = 0; \quad w = \partial b/\partial t, \quad z = b. \tag{5}$$

These are boundary conditions that state that the z-component of fluid velocity is zero (due to symmetry) at the plane of grain-to-grain contact ($z = 0$); and this component equals the velocity of the sphere surface at that surface ($z = b$). Then

$$\frac{\partial(b\rho)}{\partial t} + \int_0^b \left[\frac{\partial(\rho u)}{\partial r} + \frac{\rho u}{r}\right]\mathrm{d}z = 0. \tag{6}$$

The approximate Navier–Stokes equation for the radial flow in the contact gap is

$$\frac{\partial u}{\partial t} = -\frac{1}{\rho}\frac{\partial P}{\partial r} + \frac{\mu}{\rho}\frac{\partial^2 u}{\partial z^2}, \tag{7}$$

where μ is the dynamic viscosity. This equation is an example of the lubrication theory (e.g., Schlichting, 1951) where the z-component of the fluid velocity is neglected. It is also assumed that viscous cement is acoustic fluid and thus variations of density are small as compared to its reference value. A solution of eqn (7) in the frequency domain is

$$u(r,z) = -\frac{1}{i\omega\rho}\frac{\partial P}{\partial r}\left[1 - \frac{\cosh\left(z\sqrt{i\omega\rho/\mu}\right)}{\cosh\left(b\sqrt{i\omega\rho/\mu}\right)}\right]. \tag{8}$$

Then, and using eqns (2) and (3), we have

$$\frac{\partial(\rho u)}{\partial r} \approx \rho\frac{\partial u}{\partial r}, \quad \frac{\partial(\rho b)}{\partial t} \approx \rho\frac{\partial b}{\partial t} + \frac{b}{c_0^2}\frac{\partial P}{\partial t} = i\omega b_0\,\mathrm{e}^{i\omega t} + i\omega\,\mathrm{e}^{i\omega t}\frac{b}{c_0^2}P. \tag{9}$$

Finally, we substitute eqn (8) into eqn (6) and use eqns (2) and (9) to obtain an ordinary differential equation for pressure P in the frequency domain:

$$\left(\frac{\partial^2 P}{\partial r^2} + \frac{\partial P}{r\partial r}\right)\left(1 - \frac{\tanh\lambda}{\lambda}\right) + 2\frac{\partial P}{r\partial r}\tanh^2\lambda + P\frac{\omega^2}{c_0^2} = -\omega^2\rho b_0\frac{2R}{r^2}, \quad \lambda = \frac{r^2}{2R}\sqrt{\frac{i\omega\rho}{\mu}}. \tag{10}$$

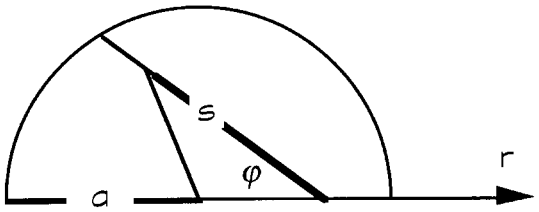

Fig. 2. Integration domain in eqn (12).

In order to find $b_0(r)$ we examine the elastic deformation of the grain surface. We use the following compatibility equation among $b_0(r)$, the elastic displacement $V(r)$ of the grain surface in the z-direction (the z-component of the displacement of the surface of the sphere relative to its center), and the rigid displacement δ of the sphere center (Dvorkin et al., 1994):

$$b_0(r) = V(r) - \delta. \tag{11}$$

Then we use an integral equation that relates $V(r)$ to pressure $P(r)$ in the viscous flow that is exerted upon the grain surface in the contact region (Timoshenko and Goodier, 1970):

$$V(r) = \frac{1-\nu}{\pi G}\int_0^{\pi} \mathrm{d}\varphi \int_0^{r\cos\varphi+\sqrt{a^2-r^2\sin^2\varphi}} P\left(\sqrt{r^2+s^2-2rs\cos\varphi}\right)\mathrm{d}s, \tag{12}$$

where ν and G are the grain Poisson's ratio and shear modulus, respectively; and a is the radius of the contact region (Fig. 1). This radius is related to the thickness h of the layer of the viscous cement around the grain as

$$a = \sqrt{2hR}. \tag{13}$$

The integration domain in eqn (12) is shown in Fig. 2.

Now by combining eqns (10)–(12), we arrive at the governing equation for pressure P:

$$\begin{aligned}&\left(\frac{\partial^2 P}{\partial r^2}+\frac{\partial P}{r\,\partial r}\right)\left(1-\frac{\tanh\lambda}{\lambda}\right)+2\frac{\partial P}{r\,\partial r}\tanh^2\lambda+P\frac{\omega^2}{c_0^2}\\ &\quad=-\omega^2\rho\frac{2R}{r^2}\left[\frac{1-\nu}{\pi G}\int_0^{\pi}\mathrm{d}\varphi\int_0^{r\cos\varphi+\sqrt{a^2-r^2\sin^2\varphi}}P\left(\sqrt{r^2+s^2-2rs\cos\varphi}\right)\mathrm{d}s-\delta\right].\end{aligned} \tag{14}$$

The boundary conditions for eqns (10) and (14) are (a) zero pressure fluctuation (from the ambient hydrostatic pressure) at the open boundary of the viscous cement layer, and (b) no flow at the center of the layer. The expressions are, respectively:

$$P = 0, \quad r = a; \quad \mathrm{d}P/\mathrm{d}r = 0, \quad r = 0. \tag{15}$$

The latter condition follows from $u = 0$ at $r = 0$ and eqn (7).

3. Numerical solution

To solve eqn (14) numerically, we first normalize it by introducing the following notations:

$$f=\frac{P}{\rho c_0^2},\quad \xi=\frac{s}{R},\quad x=\frac{r}{R},\quad \alpha=\frac{a}{R},\quad \gamma=\frac{c_0}{R\omega},\quad \lambda=\frac{x^2}{2}\sqrt{\frac{iR^2\omega\rho}{\mu}},\quad C=\frac{2\delta}{R}.$$

The resulting equation is:

$$\gamma^2\left(1-\frac{\tanh\lambda}{\lambda}\right)x^2\frac{\partial^2 f}{\partial x^2}+\gamma^2 x\left(1-\frac{\tanh\lambda}{\lambda}+2\tanh^2\lambda\right)\frac{\partial f}{\partial x}+x^2 f$$

$$=-\frac{2\rho c_0^2(1-\nu)}{\pi G}\int_0^{\pi}\mathrm{d}\varphi\int_0^{x\cos\varphi+\sqrt{a^2-x^2\sin^2\varphi}} f\left(\sqrt{x^2+\xi^2-2x\xi\cos\varphi}\right)\mathrm{d}\xi+C. \tag{16}$$

In order to find the desired normal stiffness between two grains, we relate the force acting on the grain to displacement δ. Then

$$S_{\mathrm{n}}=\frac{1}{\delta}\int_0^a P(r)2\pi r\,\mathrm{d}r=\frac{4\pi R\rho c_0^2}{C}\int_0^{\alpha} f(x)x\,\mathrm{d}x. \tag{17}$$

It is clear now that eqn (16) can be solved with an arbitrarily chosen non-zero C. The resulting normal stiffness will not depend on this choice. We solve eqn (16) using the quadrature method (e.g., Delves and Mohamed, 1985).

The results of solving eqns (16) and (17) with input parameters $G = 45$ GPa; $\nu = 0.064$; $c_0 = 1500$ m/s; $\rho = 1$ g/cm^3; $R = 10^{-4}$ m; $h = 10^{-7}$ m; $n = 9$; $\phi = 0.36$; and the dynamic viscosity of the cement 0.001 Pa s (pure water); 0.1 Pa s; and 10 Pa s are given (in terms of the real and imaginary parts of the normal stiffness S_{n}) in Fig. 3. The transition zone (from the low-frequency to high-frequency limit) of the real part of S_{n} as well as the peak of the imaginary part of S_{n} move up the frequency axis as the viscosity of the cement decreases. The frequency of this transition is inversely proportional to the viscosity of the cement.

Once S_{n} is available, we can calculate the effective bulk and shear moduli of the aggregate using eqn (1). We stress that eqn (1) has been derived for the case of static deformation of a granular aggregate.

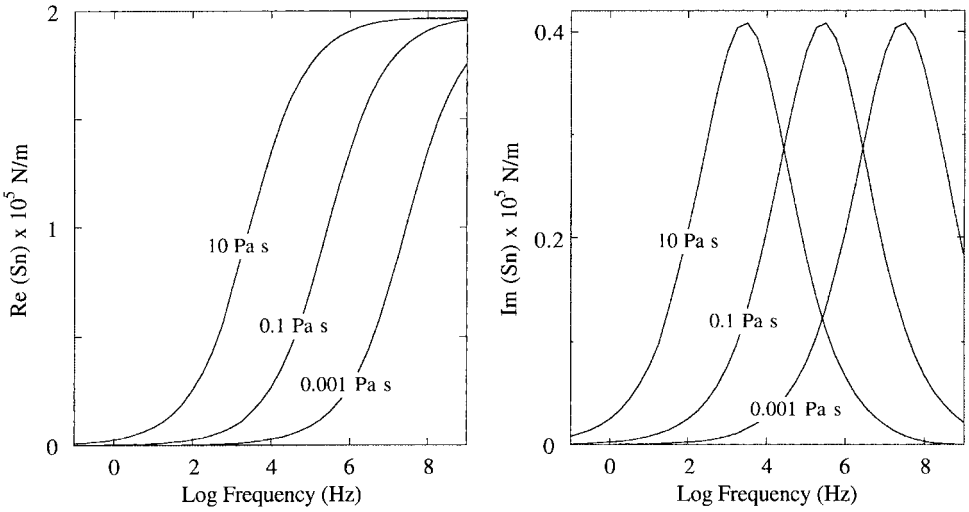

Fig. 3. Real and imaginary parts of the normal stiffness vs frequency. The dynamic viscosity of cement is given in the plots.

In the case under consideration the response of the aggregate to the load is clearly time-dependent (Fig. 3). Moreover, the imaginary part of this response is comparable in magnitude to the real part. This fact calls for a special non-static analysis of the case. In this work, we assume that eqn (1) is applicable to the case under examination.

4. Implications of solution

We use eqn (1) to find the effective bulk and shear moduli of the cemented aggregate, and then equations

$$V_{\mathrm{p}} = \sqrt{\frac{\mathrm{Re}(K_{\mathrm{Eff}} + 4G_{\mathrm{Eff}}/3)}{\rho_{\mathrm{Eff}}}}, \quad V_s = \sqrt{\frac{\mathrm{Re}(G_{\mathrm{Eff}})}{\rho_{\mathrm{Eff}}}}, \tag{18}$$

where ρ_{Eff} is the bulk density of the aggregate, to calculate compressional- and shear-wave velocities V_{p} and V_{s}. The grain density in these calculations was 2.65 g/cm^3 (quartz).

Eqn (18) gives wave velocities for the dry cemented frame of unconsolidated sediment. In order to calculate these velocities in the water-saturated sediment, we use Gassmann's (1951) equation whose applicability to the case under examination (see discussion at the end of the previous section) will be investigated later. The result for cement viscosity 10 Pa s and the saturating fluid being pure water are given in Fig. 4. The blow-ups for compressional-wave velocity are given in Fig. 5.

5. Approximate solution: Maxwell body

By carrying out the exact numerical solution for the normal stiffness in a wide range of input parameters, we find the following best-fit algebraic expressions:

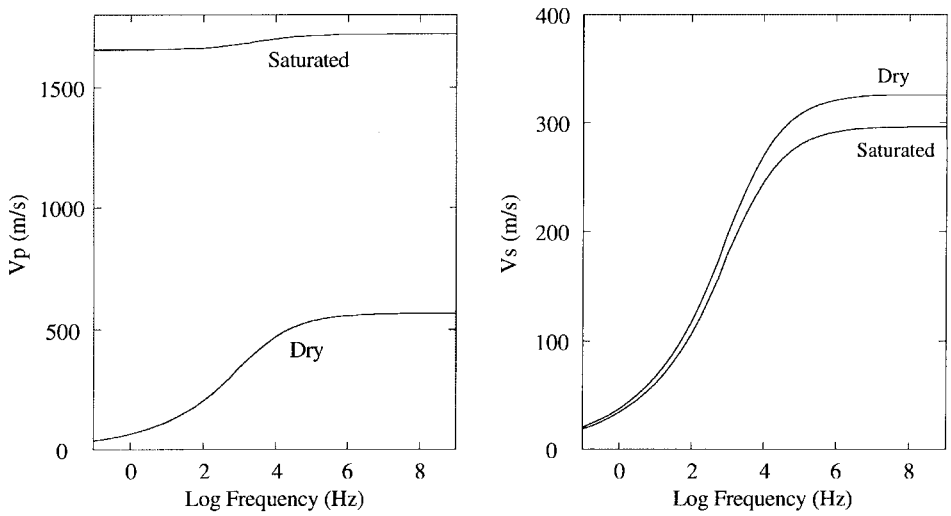

Fig. 4. Compressional- and shear-wave velocity vs frequency for dry frame and saturated sediment.

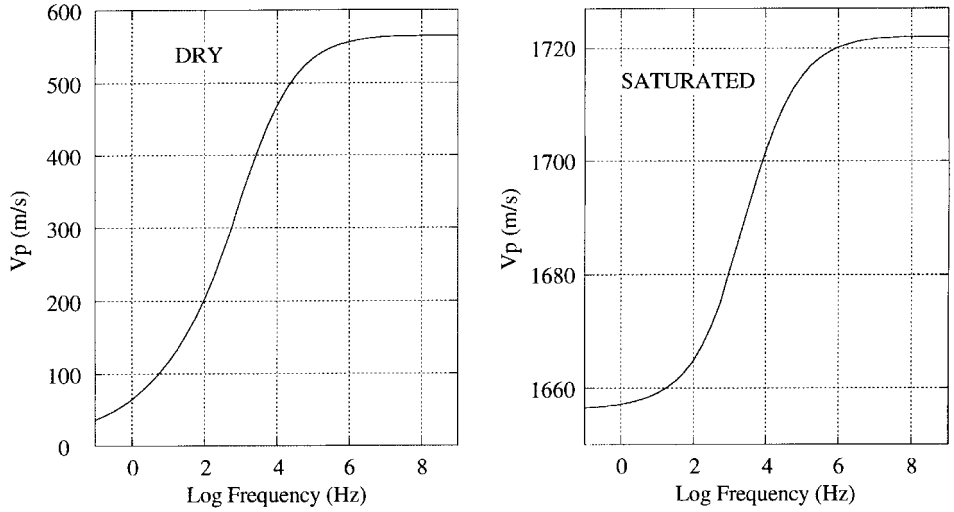

Fig. 5. Compressional-wave velocity vs frequency for dry frame and saturated sediment (blowup).

$$\frac{\mathrm{Re}(S_n)}{2\pi R\rho c_0^2} = S_\infty \frac{\omega^2\tau^2}{1+\omega^2\tau^2}; \quad \frac{\mathrm{Im}(S_n)}{2\pi R\rho c_0^2} = S_\infty \frac{\omega\tau}{1+\omega^2\tau^2}; \tag{19}$$

where

$$S_\infty = \tilde{A}\alpha^2 + \tilde{B}\alpha + \tilde{C};$$

$$\tilde{A} = 19.75 \cdot \exp(-51.9\Lambda), \quad \tilde{B} = 0.8 \cdot \Lambda^{-0.37},$$

$$\tilde{C} = -0.004 \cdot \Lambda^{-0.58}; \quad \Lambda = \rho c_0^2(1-\nu)/(\pi G); \quad \tau = 0.8\sqrt{2}\mu/\left(\rho\alpha^3 c_0^2\right). \tag{20}$$

Eqn (19) describes a Maxwell body (e.g., Bourbie et al., 1987) with the following constitutive equation:

$$\frac{\mathrm{d}\delta}{\mathrm{d}t} = \frac{F}{\eta} + \frac{1}{E}\frac{\mathrm{d}F}{\mathrm{d}t}, \tag{21}$$

where F is the contact force and δ is the corresponding displacement; and the viscoelastic constants η and E are:

$$E = 2\pi R\rho c_0^2 S_\infty, \quad \eta = 2\pi R\rho c_0^2 S_\infty \tau. \tag{22}$$

This approximate solution is compared to the exact numerical solution in Fig. 6. The high-frequency and low-frequency end members of the exact and approximate solutions are practically identical, however, the amplitude of the imaginary part of the approximate solution is about twice that of the exact solution. The reason is that the Maxwell model uses a single relaxation time which results in a narrow (in the frequency domain) transition region from the low-frequency behavior to the high-frequency behavior (Fig. 6, left).

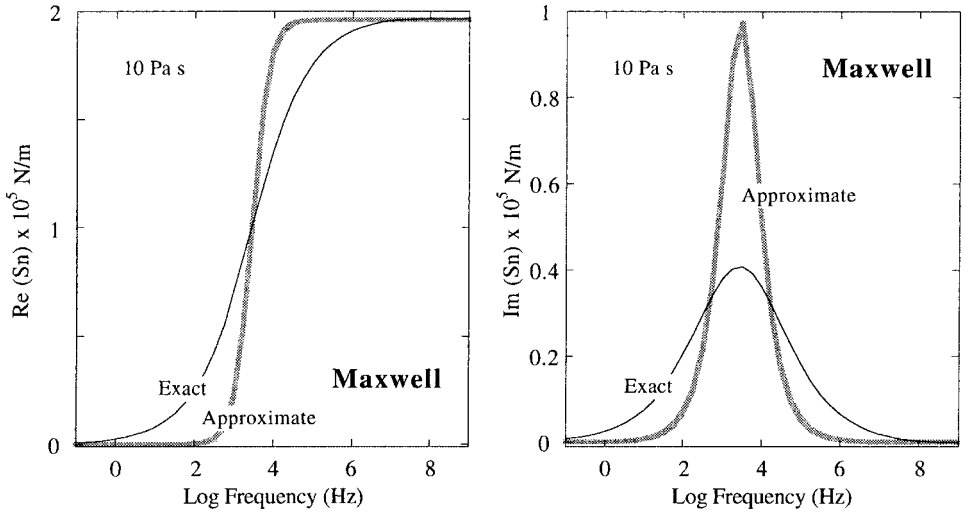

Fig. 6. Real and imaginary parts of the normal stiffness vs frequency, exact and approximate Maxwell solutions. The dynamic viscosity of cement is 10^4 Pa s.

6. Approximate solution: Cole–Cole model

A much better (than the Maxwell body) approximation to our exact numerical solution is given by the Cole–Cole (1941) model:

$$\frac{\mathrm{Re}(S_n)}{2\pi R\rho c_0^2} = S_\infty\left(1 - \frac{1+\sqrt{\omega\tau/2}}{1+\sqrt{2\omega\tau}+\omega\tau}\right); \quad \frac{\mathrm{Im}(S_n)}{2\pi R\rho c_0^2} = S_\infty\frac{\sqrt{\omega\tau/2}}{1+\sqrt{2\omega\tau}+\omega\tau}. \tag{23}$$

The results of this approximation are compared with the exact solution in Fig. 7. It can be reliably used instead of the rigorous solution.

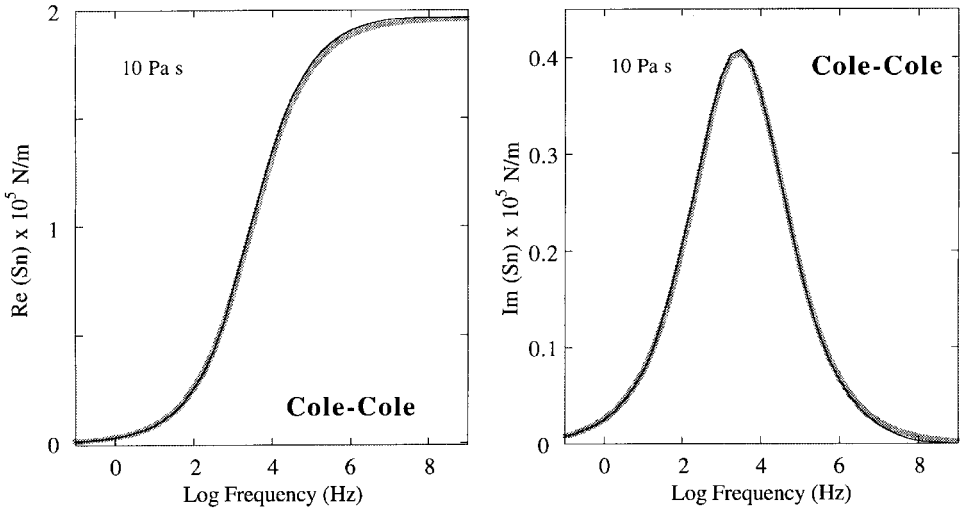

Fig. 7. Real and imaginary parts of the normal stiffness vs frequency, exact (thin dark curve) and approximate Cole–Cole (bold gray curve) solutions. The dynamic viscosity of cement is 10 Pa s.

7. Experimental verification of results

We apply our theoretical model to reproduce ultrasonic (1 MHz) experimental *P*-wave velocity measurements conducted on a dense random pack of identical glass beads partially saturated with liquid epoxy. Liquid epoxy is the state of epoxy prior to hardening. We assume here that liquid epoxy is a Newtonian fluid. The measurements have been conducted at finite confining pressure values since it was impossible (due to coupling problems) to propagate a pulse through the system at zero confining pressure. Our theoretical model, on the other hand, assumes that the grains are not precompacted.

To apply our model to the system used in the experiments, we modify it by assuming that an elastic spring is placed in parallel to the original viscoelastic model. This spring represents the finite stiffness of the system without epoxy present. As a result, we can determine the stiffness of the spring using velocity measurements at zero epoxy saturation. Then, in order to convert the experimental measurement results at a confining pressure to those without confinement, we have to subtract the elastic modulus of the dry system from that at a finite epoxy saturation.

We have available velocity measurements at 5, 10, 15, and 20 MPa confining pressure in a dry glass bead pack and in the pack with 25% epoxy saturation (Yin, 1993). In order to reproduce the experiment, we assume that the shear modulus, Poisson's ratio, and density of glass are 26.2 GPa, 0.277, and 2.48 g/cm^3, respectively (Dvorkin et al., 1994).

We did not have direct data for the viscosity, density, and the acoustic velocity in pure epoxy. We selected reasonable values of 0.5 Pa s, 1 g/cm^3, and 1500 m/s, respectively (Yin, 1993). These values allow us to consistently match the experimental data at all confining pressures (Fig. 8), which confirms the validity of our theoretical model as well as our choice of epoxy's physical properties.

In these calculations, we assumed that the epoxy evenly envelopes every grain. Therefore, the normalized contact radius α can be related to epoxy saturation s_E as (Dvorkin and Nur, 1996)

$$\alpha = \sqrt{s_E \frac{2\phi}{3(1-\phi).}} \tag{24}$$

8. Relating elastic moduli to porosity

The above results are appropriate for modeling the elastic response of an unconsolidated sediment at about 36% porosity, which is the porosity of a random pack of identical spheres. In order to extend this result for the entire porosity range, we use a model of Dvorkin and Prasad (1998) where the Hashin–Shtrikman bounds are used to calculate the dry-frame elastic moduli from those at the critical porosity. This model is based on the critical porosity concept of Nur et al. (1998). For the case under examination, critical porosity is the porosity of a dense random pack of identical spheres. Mukerji et al. (1995) show how to use this concept to modify effective medium theories for describing natural sediments. For porosity ϕ below critical porosity ϕ_c, we have

$$K_{Dry}(\phi) = \left[\frac{\phi/\phi_c}{K_{Eff} + \frac{4}{3}G_{Eff}} + \frac{1-\phi/\phi_c}{K + \frac{4}{3}G_{Eff}} \right]^{-1} - \frac{4}{3}G_{Eff},$$

$$G_{Dry}(\phi) = \left[\frac{\phi/\phi_c}{G_{Eff} + Z} + \frac{1-\phi/\phi_c}{G + Z} \right]^{-1} - Z, \quad Z = \frac{G_{Eff}}{6}\left(\frac{9K_{Eff} + 8G_{Eff}}{K_{Eff} + 2G_{Eff}} \right); \quad \phi < \phi_c, \tag{25}$$

where K_{Eff} and G_{Eff} come from eqn (1) using our sphere pack model; and K and G are the bulk and shear moduli of the grain material, respectively. For porosity above critical porosity we have

$$K_{\mathrm{Dry}} = \left[\frac{(1-\phi)/(1-\phi_c)}{K_{\mathrm{Eff}} + \frac{4}{3}G_{\mathrm{Eff}}} + \frac{(\phi-\phi_c)/(1-\phi_c)}{\frac{4}{3}G_{\mathrm{Eff}}} \right]^{-1} - \frac{4}{3}G_{\mathrm{Eff}},$$

$$G_{\mathrm{Dry}} = \left[\frac{(1-\phi)/(1-\phi_c)}{G_{\mathrm{Eff}} + Z} + \frac{(\phi-\phi_c)/(1-\phi_c)}{Z} \right]^{-1} - Z, \quad \phi > \phi_c. \tag{26}$$

The dry-frame moduli are plotted vs porosity in Fig. 9 where the parameters used are the same as for plots in Fig. 4, and frequency is infinite (elastic limit).

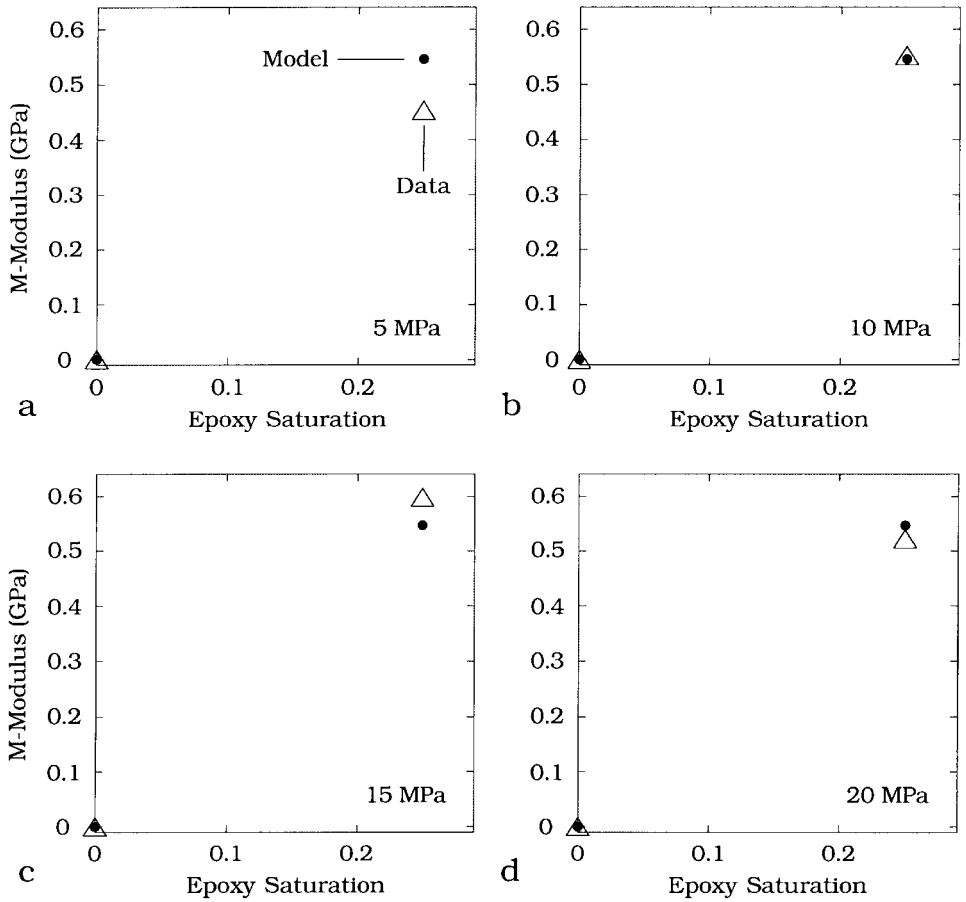

Fig. 8. Compressional-wave modulus (M-modulus) difference (saturated minus dry) of a glass-bead pack vs epoxy saturation. Triangles are the data, filled circles are from our model.

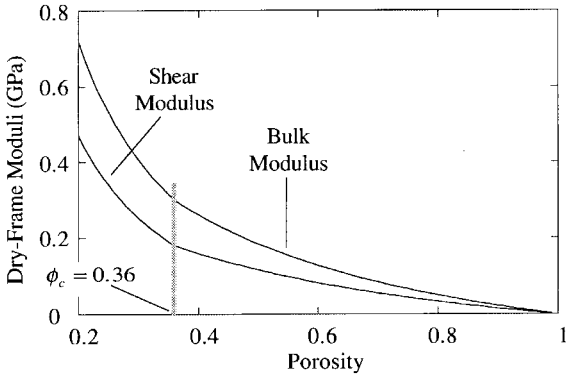

Fig. 9. Dry-frame bulk and shear moduli vs porosity calculated using eqns (25) and (26).

9. Conclusion

The theoretical model offered here is a first step towards rigorously describing the visco-elastic behavior of a particulate system with viscous cement at grain contacts. Such systems may be encountered in nature (marine sediments with clay and/or biogenic viscous matter enveloping the grains; heavy oil sands; shallow sands with viscous contaminant) and in engineering applications (asphalt concrete). The model developed here is, strictly speaking, appropriate only for suspensions with zero effective pressure. The next step is to extend this model for the case where the contacting grains are subject to a finite confining force and thus have a direct contact (Hertzian) area rather than a point contact. Such theoretical development will be accompanied by pulse-transmission experiments to measure elastic-wave velocities in relevant granular systems.

Another goal is to find an appropriate physical representation for the Cole–Cole (1941) model employed here that can be easily used in a numerical discrete element code.

In calculating the elastic moduli of the fully saturated system, we used Gassmann's (1951) equation where the dry-frame moduli are given by our model for a pack with viscous cement. We did so for simplicity. However, it is straightforward to use the Biot model instead which may help account for the global frequency dispersion in the system.

Acknowledgements

This work was supported by the Naval Research Laboratory, Stanford Rock Physics Laboratory, and the Max Kade Foundation.

References

Bourbie, T., Coussy, O., Zinszner, B., 1987. Acoustics of Porous Media. Gulf Publishing Co.

Cole, K.S., Cole, R.H., 1941. Dispersion and absorption in dielectrics. J. Chem. Phys. 9, 341–351.

Delves, L.M., Mohamed, J.L., 1985. Computational Methods for Integral Equations. Cambridge University Press.

Dvorkin, J., Mavko, G., Nur, A., 1990. The oscillations of a viscous compressible fluid in an arbitrarily-shaped pore. Mech. of Mat. 9, 165–179.

Dvorkin, J., Nur, A., Yin, H., 1994. Effective properties of cemented granular material. Mech. of Mat. 12, 207–217.

Dvorkin, J., Mavko, G., Nur, A., 1995. Squirt flow in fully saturated rocks. Geophysics 60, 97–107.

Dvorkin, J., Nur, A., 1996. Elasticity of high-porosity sandstones: Theory for two North Sea data sets. Geophysics 61, 1363–1370.
Dvorkin, J., Prasad, M., Sakai, A., Lavoie, D., 1999. Elasticity of marine sediments. GRL 26, 1781–1784.
Gassmann, F., 1951. Uber die elastizitat poroser medien (Elasticity of porous media). Vierteljahrsschrift der Naturforschenden Gesellschaft 96, 1–23.
Hashin, Z., Shtrikman, S., 1963. A variational approach to the elastic behavior of multiphase materials. J. Mech. Phys. Solids 11, 127–140.
Mavko, G., Jizba, D., 1991. Estimating grain-scale fluid effects on velocity dispersion in rocks. Geophysics 56, 1940–1949.
Mukerji, T., Berryman, J.G., Mavko, G., Berge, P.A., 1995. Differential effective medium modeling of rock elastic moduli with critical porosity constraints. Geophys. Research Letters 22, 555–558.
Nur, A., Mavko, G., Dvorkin, J., Galmudi, D., 1998. Critical porosity: a key to relating physical properties to porosity in rocks. The Leading Edge 17, 357–362.
Schlichting, H., 1951. Grenzschicht-Theorie. Karlsruhe.
Timoshenko, S.P., Goodier, J.N., 1970. Theory of Elasticity. McGraw–Hill.
Yin, H., 1993. Acoustic velocity and attenuation of rocks: isotropy, intrinsic anisotropy, and stress induced anisotropy. Ph.D. thesis, Stanford University.